# Systematic theoretical investigation of the phthalocyanine based dimer: $MnPc^{\delta+}/F_{16}CoPc^{\delta-}$

Rico Friedrich,[1] Susi Lindner,[2] Torsten Hahn,[1] Claudia Loose,[1] Simon Liebing,[1] Martin Knupfer,[2] and Jens Kortus[1,*]

[1]*Institute of Theoretical Physics, TU Bergakademie Freiberg, Leipziger Str. 23, D-09596 Freiberg, Germany*

[2]*IFW Dresden, P.O. Box 270116, D-01171 Dresden, Germany*

(Received 29 November 2012; published 18 March 2013)

In this paper, we present a systematic theoretical investigation of the phthalocyanine based dimer $MnPc^{\delta+}/F_{16}CoPc^{\delta-}$ within density functional theory framework. For all considered stacking geometries, a charge transfer from MnPc to $F_{16}CoPc$ is observed which is therefore identified as an intrinsic property of the molecular pair. In addition, a ferromagnetic coupling of the molecular magnetic moments within the dimer is always observed due to 90° superexchange and direct-exchange contributions. The comparison of the calculated absorption spectra of the different stacking arrangements to the experimentally recorded electron energy-loss spectrum strongly indicates the $\beta$ stacking to be preferred over all others. Only for this geometry an experimentally observed excitation around 0.6 eV is reproduced by the calculation.

DOI: 10.1103/PhysRevB.87.115423 PACS number(s): 71.20.Rv, 73.20.−r, 73.22.−f, 75.70.Cn

## I. INTRODUCTION

The discovery of giant magnetoresistance (GMR) in 1988 (Refs. 1 and 2) marked the start of the novel research area of spintronics. Since this time, both the scientific community as well as the types of materials investigated in view of spintronics applications have grown rapidly.[3–8] This development might offer the possibility for a spin-based electronics of the future.[9]

A novel approach to the field of spintronics was introduced in 2002 by Dediu and co-workers. They demonstrated for the first time a spin-polarized injection into an organic semiconductor by constructing an organic spin valve.[10] These devices consist of an organic spacer placed between ferromagnetic contacts and exhibit magnetoresistance according to the application of an external magnetic field. In the following years, ongoing work in the field of molecular spintronics concentrated on further development of organic spin valves.[11,12] On the other hand, experimental investigations of single molecules especially on magnetic surfaces using spin-polarized scanning tunneling microscopy and spectroscopy (STM/STS) were carried out.[13–17] These experiments were able to visualize the spin of an individual cobalt phthalocyanine molecule,[13] study the spin-polarized tunneling with intramolecular spatial resolution,[16] and demonstrate the GMR for a single molecule.[15]

Furthermore, these investigations were complemented by various theoretical studies[15–22] especially pointing out the importance of hybridization effects between molecule and substrate. Also, the inclusion of dispersion energy contributions turned out to be essential for obtaining satisfactory geometries and reliable electronic structures for molecules on surfaces.[16,23,24] Such effects have been implemented into density functional theory (DFT) either by a special functional dependence[25] or by additional dispersion corrections.[24,26–29]

Although the physical principles of the spin-polarized transport in organic spin valves remain a puzzle up to now, the decisive role of the interface between the ferromagnetic contact and the organic layer was pointed out.[30] For this finding, the special term "spinterface" was introduced by Sanvito[31] saying that the spin is manipulated right at the interface and even an inversion of the polarization due to molecule deposition on a magnetic surface can occur.[32] Recently, we demonstrated that also a spin-active interface purely made from organic components (metal phthalocyanines) can be manufactured.[33] Metal phthalocyanines (MPcs) are a class of very stable magnetic molecules[34,35] which are known since decades[36] and have been intensively investigated by various methods. They also played a major role in the STM investigations mentioned before.

The study of the phthalocyanine heterojunction utilizing x-ray photoelectron spectroscopy and DFT outlined the presence of charge transfer at the interface from manganese phthalocyanine (MnPc) to perfluorinated cobalt phthalocyanine ($F_{16}CoPc$).[33] Furthermore, the theoretical investigation suggested a ferromagnetic coupling of the magnetic moments of the molecules at the interface for the considered stacking. Therefore, the new system was called a spin-transfer material and corresponds to an extended spinterface science concept since the initial spinterface was an interface between a ferromagnetic metal (inorganic compound) and a molecular layer (organic compound).

Here, we present a systematic theoretical study of possible stacking geometries of the dimer system MnPc-$F_{16}CoPc$ based on density functional theory. This investigation seems quite important as different stackings of MPcs have been suggested either based on bulk MPc phases[37,38] or STM investigations.[39] This study suggests the probable stacking of the two types of molecules at the interface, i.e., distinguishes between the different geometries. In this framework, a theoretical investigation is particularly interesting since such geometrical relations are not easy to address experimentally as the interface is located inside the bulk.

The study of a dimer system is based on the assumption that the interaction in the interface region can be reduced to an interaction of two molecules. As it was stressed before, especially for organic $\pi$-electron systems, the van der Waals interaction is very important.[40] This can also be seen in the case of graphite where the generalized gradient approach of DFT does not predict interplanar bonding.[41] This study will show how far one can reach applying such a simple dimer model. Encouragingly, the picture associated with such a dimer model seems reasonable as also the experimental results for a coevaporated sample, where the molecules need to find each other for the interaction, exhibit the formation of the hybrid interface states.[42]

 

Our results show that the charge and spin transfer is present for every geometry and hence reveals a certain robustness of these properties against geometrical deviations. It underlines that this behavior is an intrinsic property of the molecular pair. However, the comparison of the calculated absorption spectra with the measured electron energy-loss spectrum reveals the preference of the $\beta$ stacking.

## II. COMPUTATIONAL DETAILS

The all-electron calculations within the unrestricted DFT framework were carried out using the NRLMOL program package.[43–50] The Gaussian basis set of the program was specially optimized for DFT calculations.[51] The applied exchange-correlation functionals include the local density approximation (LDA), the exchange-correlation functional of Perdew, Burke, and Ernzerhof[52] (PBE) and PBE-D2, where D2 stands for the inclusion of the dispersion correction according to Grimme.[27] For the model dimer systems consisting of MnPc and $F_{16}$CoPc, the initial geometries were based on the structures described below, and in every case the molecular planes were initially placed 3.1 Å apart from one another. This distance is in accordance with data from the Cambridge Structural Database (CSD) on $\beta$-MnPc. The presented energy-level diagrams for the different geometries have been deduced from a single-point calculation on PBE level for these initial geometries as the results show the principal interactions and hybridizations for the specific structure. Within the performed geometry optimizations with all three approaches, the initial structures were relaxed until the forces were smaller than 0.05 eV/Å.

The theoretical absorption spectra were calculated based on the electronic structure of the PBE-D2 optimized geometries from the dipole matrix elements **D** between the Kohn-Sham states. To obtain the intensities of the spectra, the transitions were weighted with $|\mathbf{D}|^2$ according to Fermi's golden rule. Moreover, a Gaussian broadening of 0.27 eV was applied to achieve comparability with the experimental resolution. To correct our data for the systematic underestimation of the band gap, which is well known for generalized gradient calculations of MPcs,[53,54] a rigid shift of the spectrum of 0.5 eV to higher energies was applied. This allowed us to align calculated and measured $Q$ band and has also been successfully applied earlier.[42,55] Such calculated absorption data can be directly compared to measured electron energy-loss spectra for small momentum transfer.[56]

## III. STACKINGS AND ELECTRONIC STRUCTURES

We start the description of the theoretical results by taking a look on the electronic and structural properties of the isolated molecular species MnPc and $F_{16}$CoPc. In the case of $F_{16}$CoPc, the characteristics are outlined in comparison to conventional CoPc. Afterwards, we will introduce the different dimer stackings as well as their specific electronic structure.

### A. Ingredients of the interface

The metal organic complex MnPc [see Fig. 1(a)] is a typical representative of a transition-metal phthalocyanine and exhibits the highest spin state $S = \frac{3}{2}$ of all common first-row transition-metal phthalocyanines.[53] Many experimental and theoretical studies have already addressed the level ordering of MnPc around the Fermi level and hence the electronic ground state of the molecule.[38,53,54,57–69] Our energy-level diagram of the compound around the Fermi level ($E_F$) has already been published,[55] and a representation including a visualization of the corresponding states can be found in the Appendix A. It is characterized by only onefold-degenerate energy levels as a distortion lifts the degeneracy of the electronic levels due to a Jahn-Teller activity[70] of the molecule.

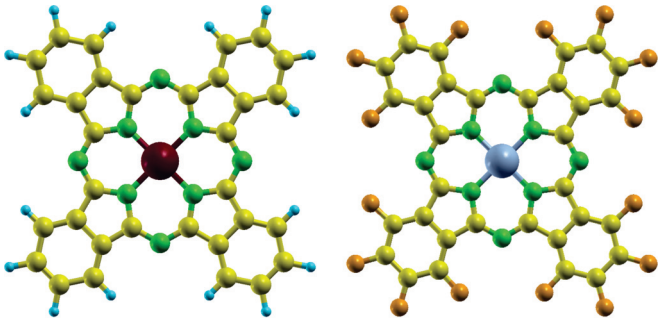

(a) (b)

FIG. 1. (Color online) Atomic structure of MnPc (a) and perfluorinated/conventional CoPc (b). The colors of the atoms correspond to the following elements: Mn = red, Co = gray, N = green, C = yellow, F/H = orange for $F_{16}$CoPc/CoPc (Ref. 79).

The metal 3*d* states mix with the ligand states around $E_F$ especially in the spin-down (minority-spin) channel. The corresponding spin-up states are considerably lower in energy due to exchange splitting. These metal states near $E_F$ are also responsible for the reduced theoretical ionization potential of MnPc of about 5.8 eV, which was calculated to be 0.5 eV lower compared to other MPcs.[55] This difference of the ionization potentials is also in very good agreement with experimental results.[69]

Now, the electronic and structural properties of perfluorinated and conventional CoPc are compared with each other to rationalize the influence of the fluorination especially on the electronic structure of the compound. Both molecular species have also been investigated by various techniques and under several conditions.[13,16,33,37,39,53,71–78] The atomic structure of both molecules is given in Fig. 1(b) and clearly pronounces the structural analogy of the systems which is also expressed by the fact that both species belong to the $D_{4h}$ point group. However, the spatial extension of the $F_{16}$CoPc molecule is slightly larger because the fluorine atoms are more extended than the hydrogen atoms in case of CoPc. Therefore, the diameter of $F_{16}$CoPc (15.7 Å) is about 0.5 Å larger than the diameter of CoPc. In both cases, the spin state is calculated to be $S = \frac{1}{2}$.

To point out the influence of the highly electronegative element fluorine clearly, the levels of both molecules in Fig. 2 are aligned at the vacuum energy $E_{\text{vac}} = 0$ (a more detailed energy-level diagram of $F_{16}$CoPc including a labeling and visualization of the states can be found in the Appendix A). One obviously identifies the striking similarity of both diagrams especially near the specific Fermi energy where the highest occupied molecular orbital (HOMO) is a ligand

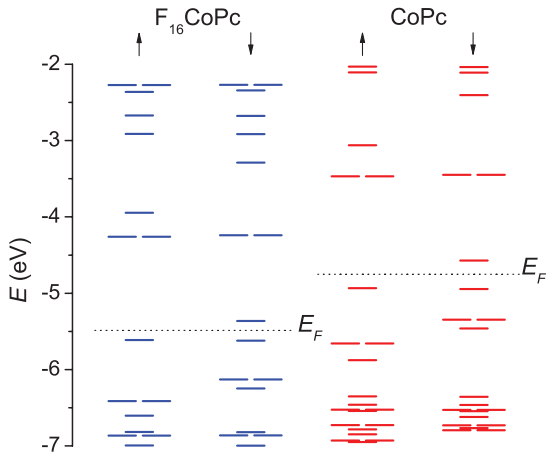


FIG. 2. (Color online) Comparison of the energy levels of $F_{16}CoPc$ and CoPc aligned at the vacuum energy. The main influence of the fluorination is an energetic downshift of the molecular levels.

derived $a_{1u}$ orbital and the lowest unoccupied molecular orbital (LUMO) is the $3d_{z^2}$ state with $a_{1g}$ symmetry at the metal center. This spin-down state is the only unoccupied metal $3d$ state at the Co and the corresponding occupied state (about 2.5 eV lower in energy due to exchange splitting) is therefore responsible for the magnetic moment of the system.

The actual influence of the fluorination is a considerable energetic lowering of the molecular states without changing the overall level alignment and orbital character. This finding is further pronounced by the computed electron affinities for both structures. This energy gain is increased from 2.9 eV in case of CoPc to 3.7 eV for the $F_{16}CoPc$ molecule.[80] Hence, the influence of the fluorination on the compound is fundamental and significantly changes its properties.

### B. Introduction of the stacking geometries

For the relative arrangement of the molecules within the dimer, different stackings are possible. On the one hand, one can deduce the geometry within the dimer from bulk MPc phases, i.e., the $\alpha$ and $\beta$ polymorphs. In the case of the $\alpha$ structure, two different modifications, namely $\alpha+$ and $\alpha\times$, were mentioned.[37,38] On the other hand, it was also deduced from STM investigations that a second phthalocyanine molecule could be placed directly on top of a first one but rotated by 45° around an axis perpendicular to the molecular plane (ontop45 stacking).[39] Either way, due to the arrangement of the molecules in the dimer structures, every symmetry present in case of the isolated systems is lifted. In the following, we describe the initial geometries a bit more in detail.

The first arrangement of the molecules to be considered is the $\beta$ stacking which is based on the $\beta$ polymorph of bulk MPcs. A visualization of the structure from side and top views is presented in Fig. 3(a). The molecules are placed over one another in such a way that the metal centers are positioned directly above or below a nitrogen atom bridging two isoindolic units of the neighboring molecule. The $\beta$-MPc phase is known to be the thermodynamically stable state for metal phthalocyanines.[35,81]

Despite the finding that the $\beta$ stacking is already capable of explaining experimental results,[33,42] also the other structures

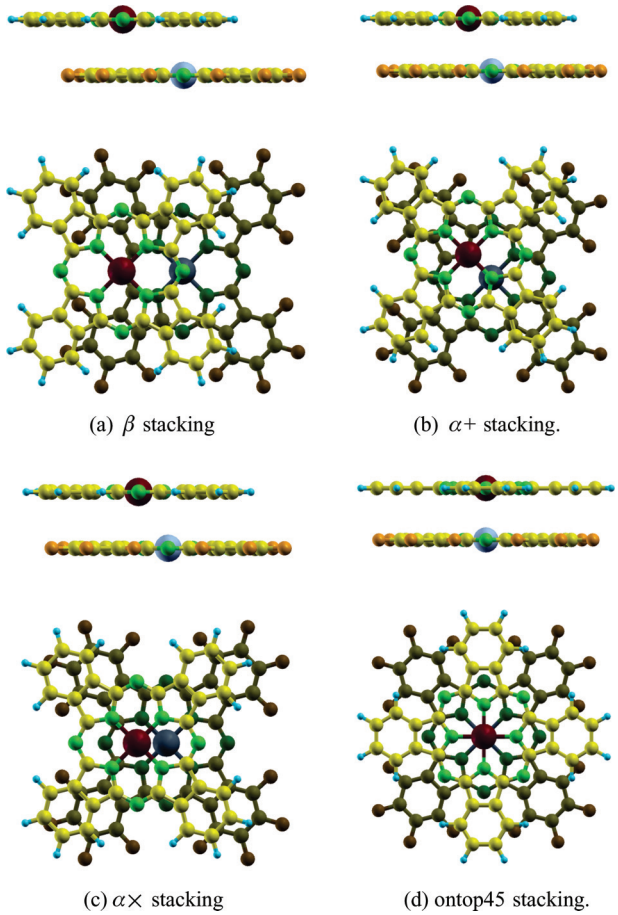


FIG. 3. (Color online) Atomic structure of the different initial dimer geometries depicted by side view (upper part) and top view (lower part) in every case. Note that the atoms of the lower molecule ($F_{16}CoPc$) in the top view are shaded.

have been investigated to clarify whether this result is robust against structural deviations and if it is possible to obtain information on the orientation of the molecules at the interface. Therefore, the next geometry to be considered is the $\alpha+$ stacking [see Fig. 3(b)]. Here, the metal centers are placed below and above a coordinating nitrogen atom of the neighboring molecule. Hence, the metal centers are closer together compared to the $\beta$ stacking (3.7 Å versus 4.6 Å).

The way in which the molecules are oriented to each other in the $\alpha\times$ stacking is shown in Fig. 3(c) and exhibits clearly that in this case the metal centers are not positioned above and below nitrogen atoms but somehow in the direction of the $\beta$ displacement. Again the metal centers are quite close to each other (3.5 Å). In the ontop45 stacking, the two molecules are placed on top of each other but rotated by 45° around an axis perpendicular to the molecular plane [see Fig. 3(d)] to avoid repulsion among the isoindolic units. Hence, the metal centers are directly on top of each other and are therefore even closer compared to the former structures (3.1 Å).

### C. Electronic structure of the $\beta$ stacking

The calculated energy-level diagram of this dimer system including the corresponding molecular orbitals is depicted in Fig. 4. It does not show degeneracy of levels due to the

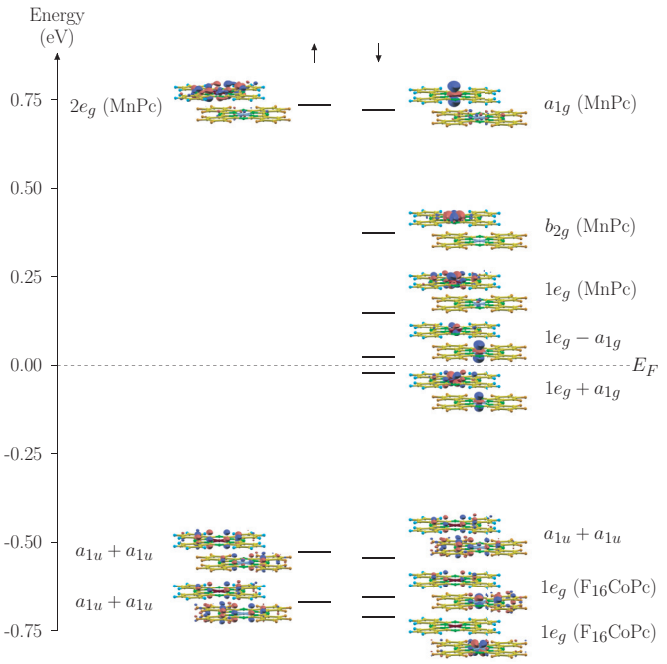


FIG. 4. (Color online) Energy-level diagram for the $\beta$ stacking. The labels of the irreducible representations refer to the states identified in correspondence to the levels of the free molecules. The according molecule is given in parentheses. If no molecule is given in brackets behind the group label, the first symbol refers to the part of the state at MnPc and the second to the part of the state at $F_{16}$CoPc. Note that the detection of hybridization is based on the observation of significant orbital contributions on both molecular structures.

lowered symmetry. Although in this new structure the states can hybridize with each other, it is still possible to identify the states of the isolated molecules as well. A detailed description of the nomenclature of the states is given in the caption of Fig. 4.

Most states within the diagram are isolated on one part of the dimer. However, as already mentioned in Ref. 33, the states close to $E_F$ show a different behavior. The $1e_g$ ($3d_{xz}$) state of MnPc hybridizes with the $a_{1g}$ ($3d_{z^2}$) state of $F_{16}$CoPc and those two form the new bonding "+" HOMO linear combination and the new antibonding "–" LUMO state of a two-level system. These two hybrid states are delocalized over the entire dimer which mediates a charge transfer from Mn to Co. In this sense, the formation of these hybrid states allowed us to explain the experimentally observed charge transfer.[33] Moreover, the binding energy of the dimer can be determined to be 7.5 eV, which includes a 2.2-eV contribution from the dispersion correction.

The theoretical value of transferred charge can be estimated based on the spin states at the metal centers to 0.2 electrons. For this purpose we used spheres of fixed radius to estimate the charge around an atom inside the sphere. However, when charge is added to a center within the dimer, a repulsion of all charge inside the sphere will result, which pushes part of the charge out of the sphere. To compensate for this complication, we looked at the magnetic moment inside the sphere as we assume both spins to be repelled equally. Therefore, a change of magnetic moment inside the sphere is indicative of a transfer of charge.

Another way to deduce the amount of transferred charge between the molecules is to calculate the charge-density difference $\rho_{\text{diff}}$, which is defined as the single-point (SCF) charge density of the dimer minus the individual charge densities of the optimized components:

$$\rho_{\text{diff}} = \rho^{\text{SCF}}_{\text{dimer}} - \rho_{F_{16}\text{CoPc}} - \rho_{\text{MnPc}}.$$

If one now takes a look at an isosurface plot of this charge-density difference [see Fig. 5(a)], bluish areas indicate where charge depletion occurs, whereas red areas represent parts where charge accumulation takes place. Obviously, the charge-density difference plot resembles the shape of the orbitals of the two-level system between which the charge is transferred, i.e., from $3d_{xz}$ to $3d_{z^2}$. Following the methodology presented in Ref. 82, the charge-density difference can be integrated to deduce the amount of charge being transferred. In Fig. 5(b), the charge-density difference integrated over the $xy$ plane is displayed along the $z$ axis which points perpendicular to the molecular planes. There, one can deduce that for the lower molecule ($F_{16}$CoPc), which is situated at $z = 0$ Å, a net charge gain occurs, whereas for the upper molecule (MnPc) at $z = 3.1$ Å, a net charge loss is observed. If now this graph is integrated for the individual molecules inside the dimer, with the according uncertainty where each molecule begins and ends, the charge transfer again amounts to about 0.2 electrons nicely confirming the estimate based on the metal

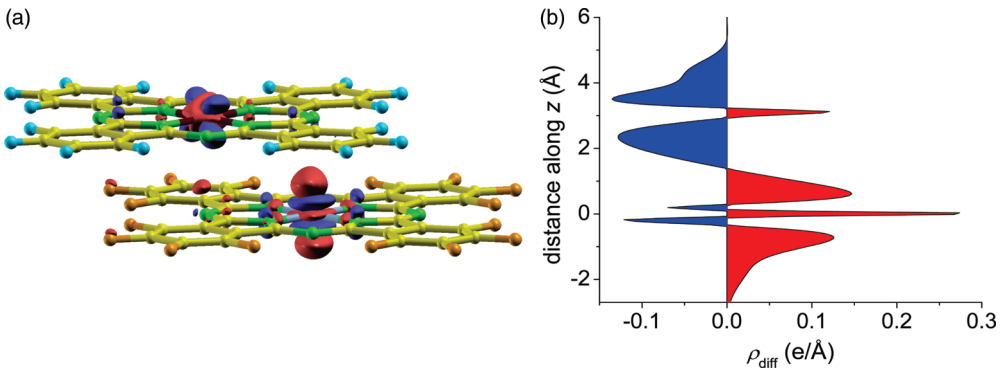


FIG. 5. (Color online) Isosurface plot of the charge-density difference $\rho_{\text{diff}}$ (a) and representation of $\rho_{\text{diff}}$ integrated over the $xy$ plane along the $z$ direction (b). Red parts denote charge accumulation, whereas blue parts indicate charge depletion.

spin states. However, the value is very sensitive to the actual distance of the molecules at the interface and the systematic underestimation of the HOMO-LUMO gap. Hence, we do not expect quantitative information from this procedure within DFT and only take it as a qualitative confirmation.

Moreover, the studied dimer has, irrespective if single-point or relaxed results are considered, a net spin of $S = 2$, which means that the two magnetic moments of the molecules couple ferromagnetically within the dimer system. This relatively high spin state makes the arrangement promising as a possible new material for spintronics as the charge transfer is accompanied by a spin transfer. The physical reason for this ferromagnetic coupling can be assigned to 90° superexchange as the two metal centers are coupled via nitrogen atoms rectangularly [see Fig. 3(a)]. The spin state of the system was carefully checked by performing additional unrestricted and restricted single-point calculations as well as geometry relaxations with an initial spin of $S = 0$ and 1 which all either relaxed to the $S = 2$ state or yielded a higher energy.

For all other geometries, a visualization of the electronic structure and a description of the specific interactions can be found in the Appendix. Also, for these geometries an interaction of the metal $3d$ states is observed. In the case of the $\alpha+$ and $\alpha\times$ stackings, the $1e_g$ ($3d_{xz}$) and $a_{1g}$ ($3d_{z^2}$) states of Mn interact with the $a_{1g}$ ($3d_{z^2}$) state of Co, whereas in case of the ontop45 stacking, the $a_{1g}$ ($3d_{z^2}$) states of both metal centers interact directly. These interactions give rise to a charge transfer which is of the same order of magnitude as in case of the $\beta$ stacking. Moreover, the ferromagnetic coupling of the molecular magnetic moments is preserved in every arrangement due to 90° superexchange and direct-exchange contributions. From this point of view, the electronic structure of the different geometries is rather similar.

### D. Comparison of the different stackings

So far, all studied arrangements were able to account for the experimentally observed charge transfer which makes this behavior an intrinsic property of the investigated molecular pair. It actually means that in every case, an interaction is present coupling the molecules and their spins in a similar way. In order to point out a physical reason why this behavior is intrinsic, in Fig. 6 the energy levels of the isolated MnPc and $F_{16}$CoPc molecules are presented next to each other aligned at the vacuum level $E_{vac} = 0$. From this comparison it is easy to see that the Fermi energy of $F_{16}$CoPc is considerably lower than that of MnPc. This is in essence due to the high electron affinity of the $F_{16}$CoPc caused by the fluorination and the low-ionization potential of MnPc originating from the split $1e_g$ states at $E_F$. Consequently, a charge transfer from MnPc to $F_{16}$CoPc within a dimer will lead to an energy gain for the electrons irrespective of the actual alignment of the molecules. In particular, as the highest occupied and lowest unoccupied states of MnPc and the LUMO of $F_{16}$CoPc are metal-derived $3d$ states, namely, $3d_{xz}$, $3d_{yz}$, and $3d_{z^2}$, the charge will be predominantly transferred between the metal centers whereas the specific interaction depends on the arrangement of the molecules as shown in the last subsection and the Appendix B. An interaction of the frontier molecular orbitals, i.e., the HOMO of the first molecule with the LUMO of the other molecule as in the $\beta$ geometry, is particularly favorable as it offers the greatest energy gain.

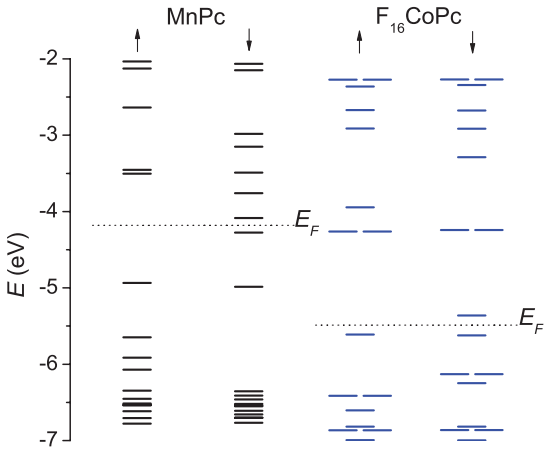


FIG. 6. (Color online) Comparison of the energy levels of MnPc and $F_{16}$CoPc aligned at the vacuum energy. The interaction of occupied states of MnPc with unoccupied states of $F_{16}$CoPc leads to an energy gain.

In order to compare the results of the different geometries and exchange-correlation functionals, Table I lists the intermolecular distance of the metal centers $d$(Mn-Co). In addition, the average molecule-molecule equilibrium distance is given in brackets behind the metal distance. The table shows the general trend of the PBE results to further enhance the intermolecular distance compared to the initial value besides for the ontop45 stacking. This expansion trend of the systems is a clear indication of the underbinding effect well known for generalized gradient approximation (GGA) calculations in general and PBE results in particular.

To consolidate this conclusion, additional LDA calculations for the systems have been carried out. As mentioned in Ref. 83, LDA calculations often yield extremely good geometries of only 1% error for bonding distances. In Table I, in all cases the distance becomes smaller during the LDA relaxation and hence the molecules come closer together. This is as expected in contrast to the PBE relaxation. Although for LDA the geometry may be reasonably good, electronic properties can be worse compared to the PBE level. Therefore, the results of the geometry optimizations in which the D2 dispersion correction of Grimme[27] (PBE-D2) was taken into account are considered. The corresponding results in Table I merely consolidate the outlined statements. For all relaxed distances, the PBE-D2 results are between the optimized LDA result

TABLE I. Distances of the metal centers $d$(Mn-Co) in Å for the geometries calculated with the different approaches. The numbers in parentheses stand for the average molecule-molecule equilibrium distances.

| Stacking | Initial | PBE | LDA | PBE-D2 |
|---|---|---|---|---|
| $\beta$ | 4.6 (3.1) | 5.1 (3.8) | 4.4 (2.8) | 4.5 (3.0) |
| $\alpha+$ | 3.7 (3.1) | 4.1 (3.7) | 2.9 (2.8) | 2.9 (2.9) |
| $\alpha\times$ | 3.5 (3.1) | 4.2 (3.8) | 2.8 (2.8) | 2.9 (2.9) |
| ontop45 | 3.1 (3.1) | 3.1 (3.1) | 2.6 (2.6) | 2.7 (2.7) |

and the initial single-point guess and they are especially very close to the single-point geometry for the $\beta$ arrangement. This finding again points to the overestimation of the intermolecular distance within the pure PBE relaxations. Hence, the results of the PBE-D2 calculations are considered to be most reliable and the spectral data shown in the next section are therefore based on these geometries.

As a final remark, at this point it is neither possible to make a clear statement on the most favorable geometry at the interface nor to exclude any geometry only based on the former investigations. Furthermore, the energy differences between the total energies and binding energies of the arrangements are for all approaches only in the range of 0.5 eV. This makes definite statements about the preferred arrangement rather complicated as this value in terms of total energies might be comparable to the error of the DFT calculation itself. Hence, one can conclude that the incompleteness of the model might play an important role. It represents the interface only by a dimer and accordingly neglects further packing effects. Such packing effects could clearly be of importance for the energetic ordering of the geometries.

## IV. CALCULATED ABSORPTION CHARACTERISTICS

In order to characterize the new phthalocyanine heterojunction further, spectroscopic measurements by means of electron energy-loss spectroscopy[56] (EELS) were performed. A description of the details and results of these measurements can be found elsewhere.[42] The striking result of this investigation was the occurrence of a new electronic excitation at 0.6 eV which could not be explained by a simple combination of the spectra of the individual MnPc and $F_{16}$CoPc species. Hence, the new signal was assigned to the formation of hybrid states.

The calculated optical absorption spectrum of the $\beta$ stacking is depicted in Fig. 7(a). One clearly sees the pronounced $Q$-band feature of the spectrum at 2 eV, which is characteristic of the whole metal phthalocyanine materials class.[55,74] The position of this peak corresponds quite good to the experimental $Q$-band region.[42] In addition to this standard signal, two more excitations occur below the $Q$ band centered at around 0.6 and 1.2 eV. Especially the first peak has quite significant intensity compared to the $Q$-band region. As one can see, the lowest signal at 0.6 eV is in nearly perfect agreement to the new experimentally observed excitation.[42]

The next geometry for which the absorption spectrum was calculated is the $\alpha+$ stacking of the dimer. In Fig. 7(b), the resulting spectrum is shown and again exhibits the pronounced $Q$-band region at the right position. However, the first strong excitation is now centered above 1.0 eV in contrast to the previous case. In conclusion, this spectrum does not correspond well to the experimental spectrum for excitation energies below 1.5 eV. The calculated spectrum for the $\alpha\times$ stacking in Fig. 7(c) again shows a dominant $Q$-band excitation around 2 eV. Moreover, also a relatively strong peak is centered at about 1.4 eV and another peak of weak intensity at about 1.1 eV is connected to this signal. From the perspective of the experimental results, there is no agreement in the energy range below 1.5 eV and in particular no strong low-lying excitation at 0.6 eV is observed. A considerably different spectral behavior compared to the former cases is found for the ontop45 stacking

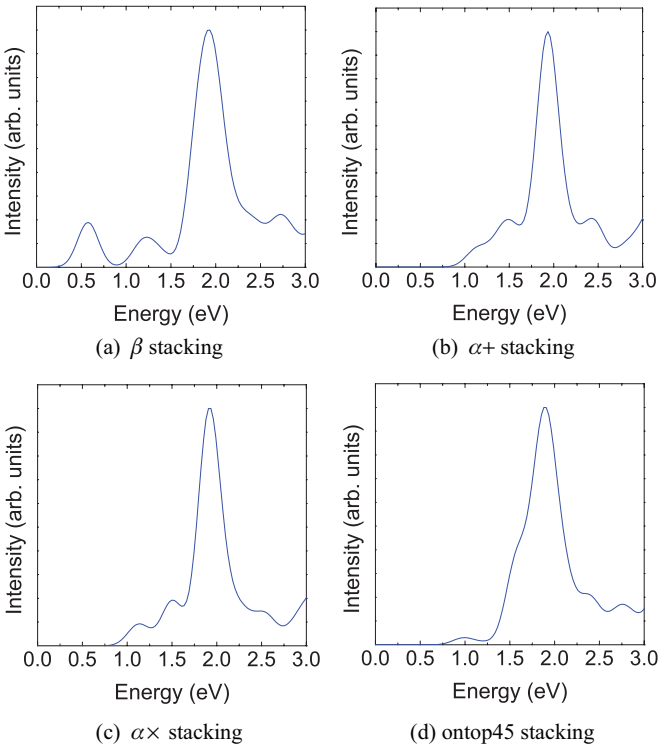


FIG. 7. (Color online) Calculated absorption spectra for the different geometries. The experimentally observed signal at 0.6 eV can only be found in the spectrum of the $\beta$ stacking.

[see Fig. 7(d)]. Here, no strong signals well below the dominant $Q$-band region are computed, and only a very small broad peak around 1.0 eV can be detected. In addition, a shoulder of the $Q$ band occurs. Therefore, the agreement with the experimental electron energy-loss spectrum is even worse compared to the former cases of the $\alpha$ geometries.

The essential conclusion is that only the spectrum of the $\beta$ stacking agrees reasonably well with the experimental results (see Fig. 8). A consideration of the underlying states of the transitions shows that the signal at 0.6 eV is caused by an intense transition between the hybrid states Mn $1e_g$ + Co $a_{1g}$ and Mn $1e_g$ − Co $a_{1g}$ of the two-level system as depicted by the inset of Fig. 8. A more detailed description of the transition states of the $\beta$ stacking can be found in Ref. 42.

For all other arrangements, fundamental differences in line shape, peak position, and intensities are calculated. In these cases, also transitions inside the corresponding two-level systems exist but as the splitting is larger, the specific signals are centered at energies above 1 eV and do not correspond to the experimental observation. Hence, the comparison with the electron energy-loss spectrum allows for the exclusion of all geometries aside from the $\beta$ arrangement, which is therefore the most probable geometrical arrangement of the molecules at the interface between MnPc and $F_{16}$CoPc. However, we can not exclude that under certain conditions, for instance the dimer deposited on a surface, a different geometry could be realized.

## V. SUMMARY

We have presented a systematic theoretical investigation of the phthalocyanine based dimer $MnPc^{\delta+}/F_{16}CoPc^{\delta-}$ using

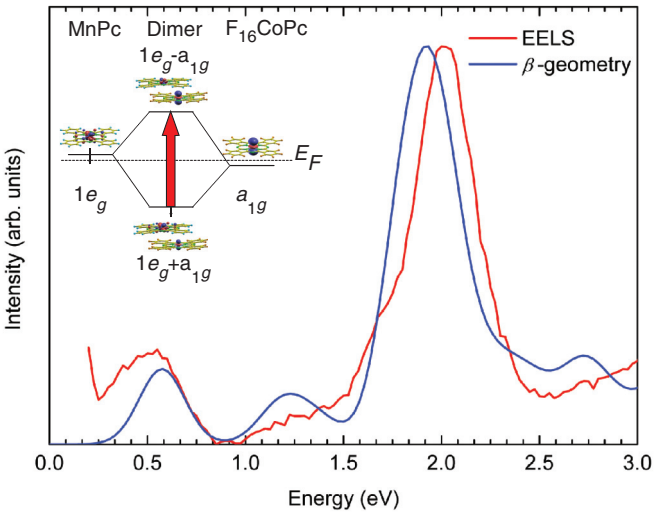


FIG. 8. (Color online) Comparison of the experimental electron energy-loss spectrum and the theoretical absorption spectrum of the $\beta$ stacking optimized with the PBE-D2 approach. The lowest signal at 0.6 eV can be assigned to a transition within the two-level system as depicted by the inset.

DFT. Within all considered stacking geometries, an intrinsic charge transfer from MnPc to $F_{16}$CoPc is calculated which can be explained by the energy-level alignment of the individual molecules. Moreover, the ferromagnetic coupling of the molecular magnetic moments within the dimer is caused by either the 90° superexchange mechanism or direct-exchange contributions. This offers a promising playground for further spintronics investigations of the system.

By the aid of further experimental investigations based on electron energy-loss spectroscopy, it was possible to deduce the $\beta$ stacking as the probable geometry at the interface since only in this case the experimental signal at 0.6 eV is theoretically reproduced. This is caused by the specific interaction mechanism in this arrangement which leads to a small splitting of the hybrid states at the Fermi level. Therefore, the introduced model has turned out to be astonishingly successful as it was not only able to clarify the principal physical effects underlying the experimental observations, but was also capable to point out the probable stacking geometry between the molecules. Finally, we would like to remark that this theoretical study is of particular importance as such geometrical relations are difficult to assess experimentally.

## ACKNOWLEDGMENTS

R.F. thanks L. Smykalla and B. Mahns for useful discussions about stacking geometries of phthalocyanine molecules. Further, we thank the Center of Information Services and High Performance Computing Dresden for computer time and support. In addition, we acknowledge financial support by the Deutsche Forschungsgemeinschaft within the Forschergruppe FOR 1154 (Towards Molecular Spintronics).

## APPENDIX A: DETAILED ENERGY-LEVEL DIAGRAMS OF MnPc AND $F_{16}$CoPc

The energy-level diagrams of individual MnPc and $F_{16}$CoPc are presented in Figs. 9 and 10. By comparing the

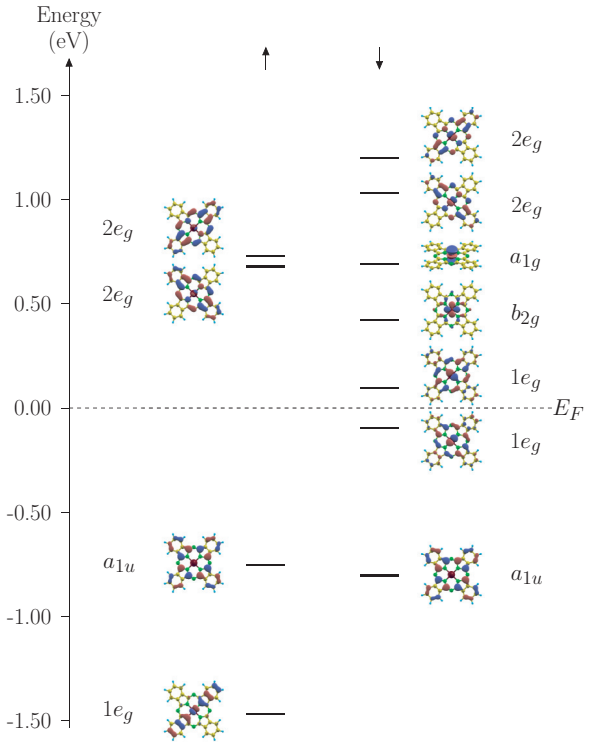


FIG. 9. (Color online) Energy-level diagram of MnPc.

diagrams, the energy-level diagrams of all dimer stackings can be understood. One can note further that the diagram of $F_{16}$CoPc exhibits additional levels (labeled with $0e_g$) well below the Fermi level compared to the diagram of CoPc. This can be attributed to the presence of the fluorine since these atoms have more electrons than hydrogen and

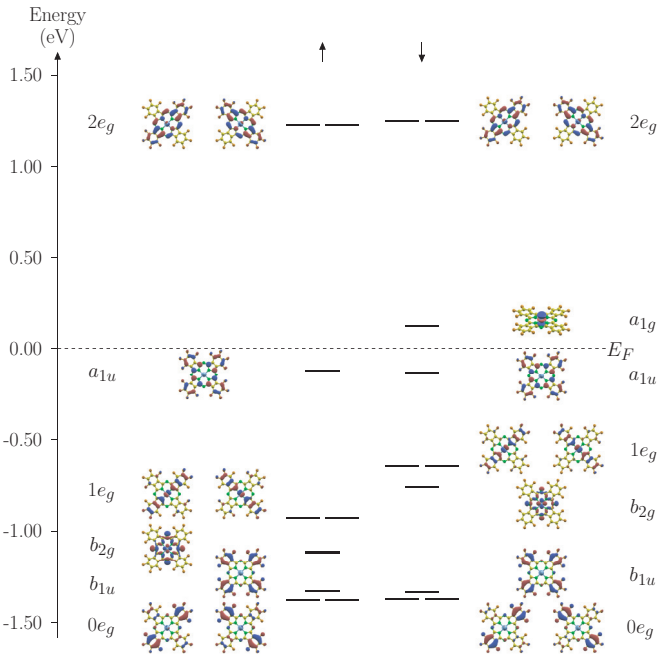


FIG. 10. (Color online) Energy-level diagram of $F_{16}$CoPc. The notation $0e_g$ for the lowest degenerate states was chosen to maintain comparability with the standard nomenclature of CoPc (Ref. 53).

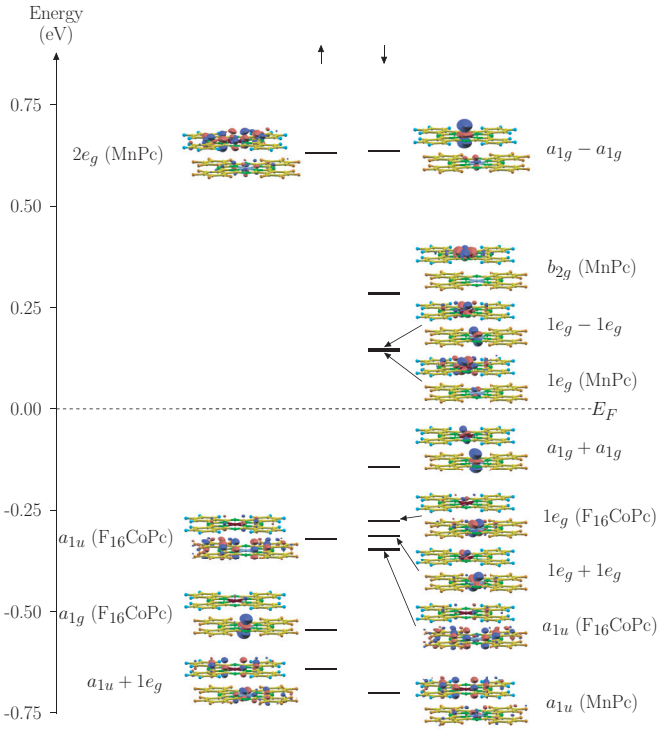


FIG. 11. (Color online) Energy-level diagram for the $\alpha+$ stacking.

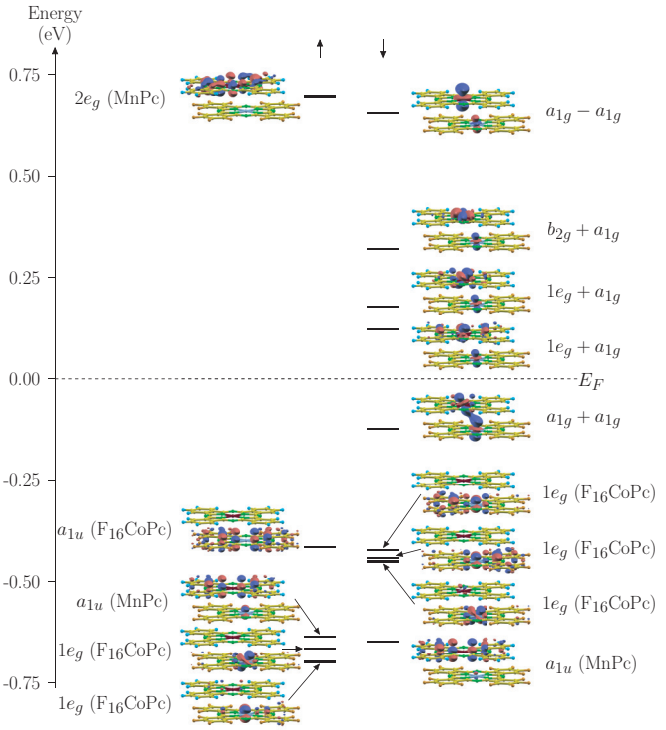


FIG. 12. (Color online) Energy-level diagram for the $\alpha\times$ stacking.

therefore will introduce additional occupied energy levels. This interpretation is supported by the fact that the additional states show orbital contributions at the fluorine atoms.

## APPENDIX B: ELECTRONIC STRUCTURES OF THE ADDITIONAL STACKINGS

### 1. Electronic structure of the $\alpha+$ stacking

The computed energy-level diagram of the $\alpha+$ stacking is presented in Fig. 11. Similar to the $\beta$ stacking, the dimer has no symmetry. Interestingly, an interaction of the molecules is still present and is now mediated by a hybridization of the $1e_g$ states and another hybridization of the $a_{1g}$ states between both molecules. This means that again the metal $3d$ orbitals of $xz$ and $z^2$ character are involved in the interactions. The $a_{1g}$ states at both molecules interact by forming a bonding linear combination $a_{1g} + a_{1g}$ that becomes the new HOMO of the system and the corresponding antibonding state $a_{1g} - a_{1g}$ that goes four states above the LUMO (LUMO + 4). In addition, also the $1e_g$ orbitals interact with each other and form a bonding state (HOMO − 4) and an antibonding state (LUMO + 1). Due to this hybridization level splittings are observed that again mediate a charge transfer into the $3d_{z^2}$ orbital of $F_{16}$CoPc, which is of the same order of magnitude as in case of the $\beta$ stacking. A similar interaction scheme has also been suggested for a CoPc dimer on a Cu(111) surface.[72]

Remarkably, the $a_{1g}$ orbitals are tilted in some cases and the $1e_g$ orbitals are polarized along one diagonal as it can for instance be seen in case of the $1e_g$ part at $F_{16}$CoPc within the HOMO − 2. This behavior is attributed to a hybridization of the $3d_{z^2}$ and $3d_{xz}$ states at each metal center. It occurs because the metal centers are close to each other but not directly on top of one another and therefore can not interact only through the $3d_{z^2}$ states due to a lack of direct overlap. Hence, a mixing with the $3d_{xz}$ function is needed to allow for a significant interaction. In order to keep notation simple, the labels next to the orbitals in the diagram were only characterized by the main angular distribution function present at each molecule.

The spin state of this arrangement is again calculated to be equal to $S = 2$, which was just like for the $\beta$ stacking thoroughly checked by additional unrestricted calculations. Again, a 90° superexchange across the bridging N is responsible for the ferromagnetic coupling of the metal centers. On the other hand, since the metal centers are much closer than in case of the $\beta$ structure, also direct exchange contributes to the ferromagnetic coupling in this case. This is underlined by the above finding that the $3d_{z^2}$ states at the metal centers hybridize and form the bonding HOMO state which indicates finite overlap between the states.

### 2. Electronic structure of the $\alpha\times$ stacking

The energy-level diagram for the $\alpha\times$ arrangement is depicted in Fig. 12. Strong hybridization within the dimer is observed for the spin-down states. As before, there is an interaction of the $a_{1g}$ states with each other leading to the bonding HOMO combination and the antibonding LUMO + 3 combination. Furthermore, there is a contribution of the $a_{1g}$ orbital of $F_{16}$CoPc to LUMO, LUMO + 1, and even LUMO + 2, which again seems to be the result of an internal hybridization of different metal $3d$ states at the Co and Mn centers. This is clearly visible in both spin channels as in the spin-up channel the HOMO − 7 ($1e_g$ state at $F_{16}$CoPc) is polarized along the bluish lobes of the orbital. In the spin-down channel the tilting of the $1e_g$ part of the LUMO + 1 at the MnPc also reveals such a mixing with different $3d$ states

at the Mn. Nevertheless, the main interaction is mediated via the $a_{1g}$ states and again causes a charge transfer of the known order. Interestingly, in the spin-down channel the $1e_g$ state of $F_{16}CoPc$ mixes inside the $F_{16}CoPc$ molecule with the $a_{1u}$ which leads to the HOMO $-$ 2 and HOMO $-$ 3. As the main contribution in both cases was deduced to be of $1e_g$ character, these two states are labeled with only this irreducible representation.

The spin state of the system was as in the former two cases verified by several test calculations and amounts to $S = 2$ for the single point and the optimization calculations as well. Since as described above no 90° exchange path between the metal centers through nitrogen atoms exists in this arrangement, 90° superexchange can actually be excluded as the underlying exchange mechanism. Due to the proximity of the metal atoms, the direct-exchange mechanism as the dominant contribution for the ferromagnetic coupling of the magnetic moments seems likely and is supported by the detected $a_{1g}$ interaction for the HOMO. This leads to the conclusion that the computed spin state is relatively robust towards small geometrical deviations inside the dimer as different magnetic interaction mechanisms seem to favor the ferromagnetic alignment.

### 3. Electronic structure of the ontop45 stacking

The energy-level diagram of the ontop45 stacking presented in Fig. 13 exhibits clearly that most of the states are localized on either only the MnPc or only the $F_{16}CoPc$ of the dimer. However, a strong interaction and hybridization of the $a_{1g}$ states of the molecules is observed which is now possible without internal polarization as the metal centers are suitably arranged. The bonding combination of the interaction in the spin-down channel becomes the HOMO $-$ 4 and the antibonding combination is destabilized to such an extent that it is not visible in the depicted energy range above the Fermi level. In the spin-up channel the antibonding combination is clearly identified as the HOMO $-$ 8, whereas the bonding combination is well below $E_F$ and not shown in the depicted energy range

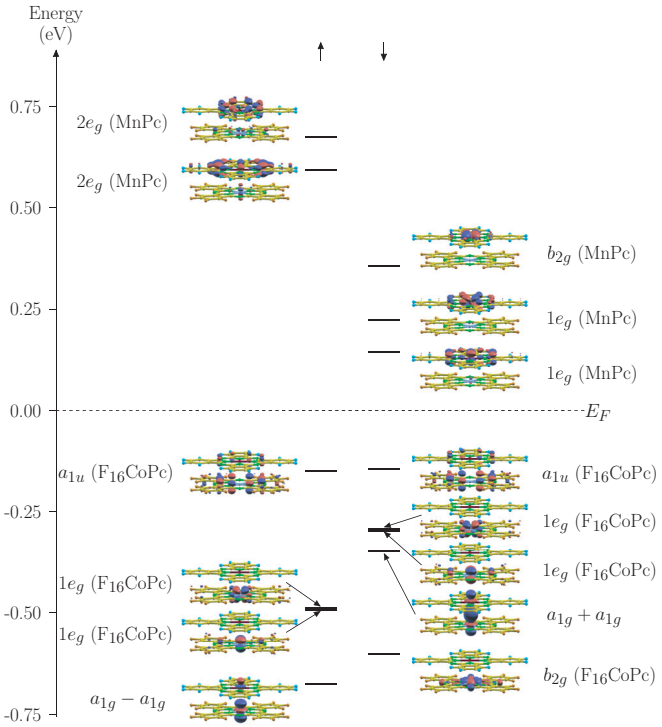


FIG. 13. (Color online) Energy-level diagram for the ontop45 stacking.

of Fig. 13. The interaction of the states causes again the known charge-transfer phenomenon as the electron from the singly occupied $1e_g$ state of MnPc is transferred into the bonding $a_{1g}$ hybrid state.

For all types of calculations, the spin state of $S = 2$ was validated carefully. In the present arrangement, the ferromagnetic alignment of the magnetic moments due to direct exchange seems most likely again, which is further confirmed by the observed bonding of the $3d_{z^2}$ states (HOMO $-$ 4).

*jens.kortus@physik.tu-freiberg.de

[1] M. N. Baibich, J. M. Broto, A. Fert, F. Nguyen Van Dau, F. Petroff, P. Etienne, G. Creuzet, A. Friederich, and J. Chazelas, Phys. Rev. Lett. **61**, 2472 (1988).
[2] G. Binasch, P. Grünberg, F. Saurenbach, and W. Zinn, Phys. Rev. B **39**, 4828 (1989).
[3] G. A. Prinz, Science **282**, 1660 (1998).
[4] I. Zutic, J. Fabian, and S. Das Sarma, Rev. Mod. Phys. **76**, 323 (2004).
[5] H. Munekata, I. Zutic, J. Fabian, S. Tarucha, M. Stopa, S. Sasaki, K. Ono, J. Martinek, J. Barnas, D. C. Ralph, R. A. Buhrman, X. Jiang, S. Parkin, E. Barnes, S. Maekawa, S. Takahashi, H. Imamura, and S. Maekawa, *Concepts in Spin Electronics*, edited by S. Maekawa ( Oxford University Press, Oxford, UK, 2006).
[6] S. Sanvito, J. Mater. Chem. **17**, 4455 (2007).
[7] S. Sanvito, Nat. Mater. **6**, 803 (2007).
[8] A. Fert, Rev. Mod. Phys. **80**, 1517 (2008).
[9] S. Wolf and D. Awschalom, Science **294**, 1488 (2001).
[10] V. Dediu, M. Murgia, F. Matacotta, C. Taliani, and S. Barbanera, Solid State Commun. **122**, 181 (2002).
[11] Z. H. Xiong, D. Wu, Z. V. Vardeny, and J. Shi, Nature (London) **427**, 821 (2004).
[12] M. Shiraishi and T. Ikoma, Phys. E (Amsterdam) **43**, 1295 (2011).
[13] C. Iacovita, M. V. Rastei, B. W. Heinrich, T. Brumme, J. Kortus, L. Limot, and J. P. Bucher, Phys. Rev. Lett. **101**, 116602 (2008).
[14] N. Tsukahara, K.-i. Noto, M. Ohara, S. Shiraki, N. Takagi, Y. Takata, J. Miyawaki, M. Taguchi, A. Chainani, S. Shin, and M. Kawai, Phys. Rev. Lett. **102**, 167203 (2009).
[15] S. Schmaus, A. Bagrets, Y. Nahas, T. K. Yamada, A. Bork, M. Bowen, E. Beaurepaire, F. Evers, and W. Wulfhekel, Nat. Nanotechnol. **6**, 185 (2011).
[16] J. Brede, N. Atodiresei, S. Kuck, P. Lazic, V. Caciuc, Y. Morikawa, G. Hoffmann, S. Blügel, and R. Wiesendanger, Phys. Rev. Lett. **105**, 047204 (2010).
[17] N. Atodiresei, J. Brede, P. Lazic, V. Caciuc, G. Hoffmann, R. Wiesendanger, and S. Blügel, Phys. Rev. Lett. **105**, 066601 (2010).

[18]E. G. Emberly and G. Kirczenow, Chem. Phys. **281**, 311 (2002).
[19]A. R. Rocha, V. M. Garcia-Suarez, S. W. Bailey, C. J. Lambert, J. Ferrer, and S. Sanvito, Nat. Mater. **4**, 335 (2005).
[20]D. Waldron, P. Haney, B. Larade, A. MacDonald, and H. Guo, Phys. Rev. Lett. **96**, 166804 (2006).
[21]S. Sanvito and A. Rocha, J. Comput. Theor. Nanosci. **3**, 624 (2006).
[22]A. R. Rocha and S. Sanvito, J. Appl. Phys. **101**, 09B102 (2007).
[23]N. Atodiresei, V. Caciuc, P. Lazic, and S. Blügel, Phys. Rev. Lett. **102**, 136809 (2009).
[24]V. G. Ruiz, W. Liu, E. Zojer, M. Scheffler, and A. Tkatchenko, Phys. Rev. Lett. **108**, 146103 (2012).
[25]M. Dion, H. Rydberg, E. Schröder, D. C. Langreth, and B. I. Lundqvist, Phys. Rev. Lett. **92**, 246401 (2004).
[26]S. Grimme, J. Comput. Chem. **25**, 1463 (2004).
[27]S. Grimme, J. Comput. Chem. **27**, 1787 (2006).
[28]A. Tkatchenko and M. Scheffler, Phys. Rev. Lett. **102**, 073005 (2009).
[29]S. Grimme, J. Antony, S. Ehrlich, and H. Krieg, J. Chem. Phys. **132**, 154104 (2010).
[30]C. Barraud, P. Seneor, R. Mattana, S. Fusil, K. Bouzehouane, C. Deranlot, P. Graziosi, L. Hueso, I. Bergenti, V. Dediu, F. Petroff, and A. Fert, Nat. Phys. **6**, 615 (2010).
[31]S. Sanvito, Nat. Phys. **6**, 562 (2010).
[32]S. Sanvito, Nature (London) **467**, 664 (2010).
[33]S. Lindner, M. Knupfer, R. Friedrich, T. Hahn, and J. Kortus, Phys. Rev. Lett. **109**, 027601 (2012).
[34]C. G. Claessens, U. Hahn, and T. Torres, Chem. Record **8**, 75 (2008).
[35]Z. Ni, R. Li, and J. Jiang, *Controlled Assembly and Modification of Inorganic Systems*, Vol. 133 ( Springer, Berlin, 2009), pp. 121–160.
[36]R. Linstead, J. Chem. Soc. (1934) 1016.
[37]M. Takada and H. Tada, Chem. Phys. Lett. **392**, 265 (2004).
[38]W. Wu, A. Kerridge, A. H. Harker, and A. J. Fisher, Phys. Rev. B **77**, 184403 (2008).
[39]X. Chen, Y.-S. Fu, S.-H. Ji, T. Zhang, P. Cheng, X.-C. Ma, X.-L. Zou, W.-H. Duan, J.-F. Jia, and Q.-K. Xue, Phys. Rev. Lett. **101**, 197208 (2008).
[40]S. Braun, W. R. Salaneck, and M. Fahlman, Adv. Mater. **21**, 1450 (2009).
[41]N. Ooi, A. Rairkar, and J. B. Adams, Carbon **44**, 231 (2006).
[42]S. Lindner, B. Mahns, A. König, F. Roth, M. Knupfer, R. Friedrich, T. Hahn, and J. Kortus, J. Chem. Phys. **138**, 024707 (2013).
[43]M. R. Pederson and K. A. Jackson, Phys. Rev. B **41**, 7453 (1990).
[44]K. A. Jackson and M. R. Pederson, Phys. Rev. B **42**, 3276 (1990).
[45]M. R. Pederson and K. A. Jackson, Phys. Rev. B **43**, 7312 (1991).
[46]A. Quong, M. Pederson, and J. Feldman, Solid State Commun. **87**, 535 (1993).
[47]D. Porezag and M. R. Pederson, Phys. Rev. B **54**, 7830 (1996).
[48]D. Porezag, Ph.D. thesis, Technische Universität Chemnitz-Zwickau, 1997.
[49]A. Briley, M. R. Pederson, K. A. Jackson, D. C. Patton, and D. V. Porezag, Phys. Rev. B **58**, 1786 (1998).
[50]M. Pederson, D. Porezag, J. Kortus, and D. Patton, Phys. Status Solidi B **217**, 197 (2000).
[51]D. Porezag and M. R. Pederson, Phys. Rev. A **60**, 2840 (1999).
[52]J. P. Perdew, K. Burke, and M. Ernzerhof, Phys. Rev. Lett. **77**, 3865 (1996).
[53]X. Shen, L. Sun, Z. Yi, E. Benassi, R. Zhang, Z. Shen, S. Sanvito, and S. Hou, Phys. Chem. Chem. Phys. **12**, 10805 (2010).
[54]X. Shen, L. Sun, E. Benassi, Z. Shen, X. Zhao, S. Sanvito, and S. Hou, J. Chem. Phys. **132**, 054703 (2010).
[55]R. Friedrich, T. Hahn, J. Kortus, M. Fronk, F. Haidu, G. Salvan, D. R. T. Zahn, M. Schlesinger, M. Mehring, F. Roth, B. Mahns, and M. Knupfer, J. Chem. Phys. **136**, 064704 (2012).
[56]J. Fink, Adv. Electron. Electron Phys. **75**, 121 (1989).
[57]C. G. Barraclough, R. L. Martin, S. Mitra, and R. C. Sherwood, J. Chem. Phys. **53**, 1638 (1970).
[58]A. M. Schaffer, M. Gouterman, and E. R. Davidson, Theor. Chim. Acta **30**, 9 (1973).
[59]S. Mitra, A. K. Gregson, W. E. Hatfield, and R. R. Weller, Inorg. Chem. **22**, 1729 (1983).
[60]P. A. Reynolds and B. N. Figgis, Inorg. Chem. **30**, 2294 (1991).
[61]B. E. Williamson, T. C. VanCott, M. E. Boyle, G. C. Misener, M. J. Stillman, and P. N. Schatz, J. Am. Chem. Soc. **114**, 2412 (2012).
[62]T. Suzuki, M. Kurahashi, X. Ju, and Y. Yamauchi, J. Phys. Chem. B **106**, 11553 (2002).
[63]N. Papageorgiou, E. Salomon, T. Angot, J.-M. Layet, L. Giovanelli, and G. L. Lay, Prog. Surf. Sci. **77**, 139 (2004).
[64]A. Calzolari, A. Ferretti, and M. B. Nardelli, Nanotechnology **18**, 424013 (2007).
[65]R. Kraus, M. Grobosch, and M. Knupfer, Chem. Phys. Lett. **469**, 121 (2009).
[66]D. Stradi, C. Diaz, F. Martin, and M. Alcami, Theor. Chem. Acc. **128**, 497 (2010).
[67]M.-S. Liao, J. D. Watts, and M.-J. Huang, Inorg. Chem. **44**, 1941 (2005).
[68]N. Marom and L. Kronik, Appl. Phys. A **95**, 165 (2008).
[69]M. Grobosch, B. Mahns, C. Loose, R. Friedrich, C. Schmidt, J. Kortus, and M. Knupfer, Chem. Phys. Lett. **505**, 122 (2011).
[70]H. Jahn and E. Teller, Proc. R. Soc. London, Ser. A **161**, 220 (1937).
[71]L. Scudiero, K. W. Hipps, and D. E. Barlow, J. Phys. Chem. B **107**, 2903 (2003).
[72]X. Ge, C. Manzano, R. Berndt, L. T. Anger, F. Köhler, and R. Herges, J. Am. Chem. Soc. **131**, 6096 (2009).
[73]D. G. de Oteyza, E. Barrena, Y. Zhang, T. N. Krauss, A. Turak, A. Vorobiev, and H. Dosch, J. Phys. Chem. C **113**, 4234 (2009).
[74]M. Grobosch, C. Schmidt, R. Kraus, and M. Knupfer, Org. Electron. **11**, 1483 (2010).
[75]M. Toader, T. G. Gopakumar, M. Abdel-Hafiez, and M. Hietschold, J. Phys. Chem. C **114**, 3537 (2010).
[76]M. Toader, T. G. Gopakumar, P. Shukrynau, and M. Hietschold, J. Phys. Chem. C **114**, 21548 (2010).
[77]S. Lindner, U. Treske, M. Grobosch, and M. Knupfer, Appl. Phys. A **105**, 921 (2011).
[78]M. Toader, M. Knupfer, D. R. Zahn, and M. Hietschold, Surf. Sci. **605**, 1510 (2011).
[79]A. Kokalj, Comput. Mater. Sci. **28**, 155 (2003).
[80]Note that these values are calculated such that the structure of the compound with the additional electron was relaxed and the energy difference to the total energy of the neutral system was deduced afterwards.
[81]J. H. Beynon and A. R. Humphries, Trans. Faraday Soc. **51**, 1065 (1955).
[82]G. Heimel, L. Romaner, J.-L. Bredas, and E. Zojer, Surf. Sci. **600**, 4548 (2006).
[83]W. Kohn, Rev. Mod. Phys. **71**, 1253 (1999).